Scientific African 19 (2023) e01490

Contents lists available at ScienceDirect

Scientific African

journal homepage: www.elsevier.com/locate/sciaf

Adaptive techniques for solving chaotic system of parabolic-type

Kolade M. Owolabi[a,*], Edson Pindza[b]

[a] Department of Mathematical Sciences, Federal University of Technology, Akure, PMB 704, Ondo State, Nigeria
[b] Department of Mathematics and Applied Mathematics, University of Pretoria, Pretoria 002, South Africa

ARTICLE INFO

Article history:
Received 3 July 2022
Revised 21 October 2022
Accepted 6 December 2022

Editor DR B Gyampoh

2010 MSC:
26A33
34A34
35A05
35K57
65L05
65M06
93C10

Keywords:
Exponential time-differencing method
Numerical simulations
Reaction-diffusion equations
Spatiotemporal patterns
Spectral method

ABSTRACT

Time-dependent partial differential equations of parabolic type are known to have a lot of applications in biology, mechanics, epidemiology and control processes. Despite the usefulness of this class of differential equations, the numerical approach to its solution, especially in high dimensions, is still poorly understood. Since the nature of reaction-diffusion problems permit the use of different methods in space and time, two important approximation schemes which are based on the spectral and barycentric interpolation collocation techniques are adopted in conjunction with the third-order exponential time-differencing Runge-Kutta method to advance in time. The accuracy of the method is tested by considering a number of time-dependent reaction-diffusion problems that are still of current and recurring interests in one and high dimensions.

Introduction

Most meaningful practical and real-life problems such as Burgers, Robertson, Fisher, Gray-Scott, Allen-Cahn, Korteweg-de Vries (KdV), Schrodinger, Kadomtsev-Petviashvili, Kuramoto–Sivashinsky, Navier-Stokes, Davey-Stewartson equations, among many others which are often encountered in engineering and applied sciences exist in the form of partial differential equations (PDEs) [1–5]. Mathematical modelling of various physical scenarios in applied mathematics and ecology which include pattern formation process, elasticity, hydrodynamics, electromagnetic theory, nonlinear optics, acoustics, plasma physics, Bose-Einstein condensates, and quantum mechanics among others, also involves PDEs.

Due to nonlinearity nature of the type of chaotic or dispersive equations [6], to obtain their analytical solutions is almost impossible, and where it is possible it may requires rigorous mathematical techniques to obtain a solution. In view

* Corresponding author.
E-mail address: kmowolabi@futa.edu.ng (K.M. Owolabi).

https://doi.org/10.1016/j.sciaf.2022.e01490

of the importance of these equations and the open mathematical questions that may arise, efficient and robust numerical algorithms are required to enable extensive numerical studies of the PDEs.

A specific interest of study in this paper is the parabolic-type of PDE which has been used to describe a variety of time-dependent phenomena such as wave propagation, particle diffusion, heat conduction, ocean acoustic propagation, and pricing of derivative investment instruments [7,8].

Over the last few decades, much attention has been given to the challenges of finding numerical solution to this class of time-dependent parabolic PDEs [1,9,10]. However, a number of numerical methods have been proposed for finding the approximate solutions for this class of differential equations written in the form

$$u_t = \mathcal{L}u + \mathcal{F}(u,t) \tag{1}$$

where $\mathcal{L}$ and $\mathcal{F}$ (which represents the biological or chemical reaction kinetics) denote the linear and nonlinear operators, respectively.

The coupled reaction-diffusion equations take the form

$$(u_i)_t = d_i \mathbf{L}_i u_i + f_i(t,x,u_i), \qquad i = 1,2,\ldots, \quad t \in (0,T], \quad x \in \Omega \tag{2}$$

subject to the boundary and initial conditions

$$\frac{\partial u_i}{\partial \boldsymbol{\nu}} = 0, \quad u_i(0,x) = \alpha_i(x), \quad \text{for } 1,2,\ldots \quad t \in (0,T], \quad x \in \Omega \tag{3}$$

where d_i is the diffusion coefficients of species u_i for $i = 1,2,\ldots$, Ω is the bounded domain in $\mathbf{R}^n$ $(n = 1,2,\ldots)$, $\partial\Omega$ is the boundary of Ω, $\partial/\partial\boldsymbol{\nu}$ is the outward normal derivative on $\partial\Omega$.

In reality, many time-dependent PDEs as in (1) combines low-order nonlinear parts with the higher-order linear parts. When (1) is discretized in space with either finite difference or spectral methods, one obtains a system of coupled linear ordinary differential equations in time. The resulting system of ODEs is known to be stiff [11,12]. The linear parts are primarily responsible for the stiffness with rapid exponential decay of some modes or a rapid oscillation of some modes, as with the case of a chaotic or dissipative PDEs, respectively.

The traditional way of solving this type of problems is by applying the known finite difference method, finite-element method, finite volume method, and Fourier spectral method [13–17]. There are other approaches which had been applied to deal precisely with the equations of the form (1) with a linear stiff term as implicit-explicit (IMEX) scheme [18–20], time splitting and integrating factor (IF) schemes [21] as well as sliders and exponential time differencing [11,22,23]. B-spline collocation method has been used to solve many PDEs [24,25]. Likewise the meshless barycentric interpolation collocation method had solved a range of elliptic and parabolic PDEs [26,27]. Apart from the methods discussed here, a number of numerical techniques which has been applied to solve time-dependent PDEs can be found in [28–31], and references therein. This work adapts two trending numerical schemes that are based on the spectral and barycentric interpolation collocation methods in conjunction with the novel third-order exponential time differencing Runge-Kutta scheme to explore high dimensional patterns in time-dependent reaction-diffusion problems of parabolic type.

The remainder part of this paper is organized as follows. Some preliminaries such as definitions and useful results are presented in Section 2. The main numerical methods in space and time and described in Section 3 with numerical example to justify their suitability. Several numerical examples such as the Allen-Cahn bistable equation and coupled predator-prey model are experimented in Section 4 with a view to explore their dynamic richness in one, two and three dimensional spaces. Conclusion is finally drawn with the last section.

Preliminaries

In this section, some useful definitions and results are briefly reported. Barycentric interpolation collocation method is known to be of high precision and efficiency numerical scheme for solving linear differential equations. In most cases where BICM is applied, the nonlinear terms are converted to linear differential equations. Recall that the general time-dependent problem (1) can be broken into linear and nonlinear terms as

$$\mathscr{L}u(x,t) + \mathscr{F}u(x,t) = f(x,t) \tag{4}$$

where $\mathscr{L}$ and $\mathscr{F}$ represent the operator for the linear and nonlinear terms, respectively, and $f(x,t)$ is any local kinetic. Assuming $u_0(x,t)$ is given, then the above equation becomes

$$\mathscr{L}u(x,t) + \mathscr{F}u_0(x,t) = f(x,t) \tag{5}$$

which means that (4) has been transformed to a linear equation as in (5). It is possible to obtain a new function $u_1(x,t)$ for solving (5), and have a linear iterative method

$$\mathscr{L}u_n(x,t) + \mathscr{F}u_{n-1}(x,t) = f(x,t). \tag{6}$$

If $u_n(x,t) \to u(x,t)$ as $n \to \infty$, we say that the linear iterative method (6) is convergent.

Theorem 2.1 *[32]. Suppose that the linear operator $\mathscr{L}$ is bounded, and $\mathscr{F}$ is a Frechet differentiable operator. If the exact and numerical solution of (1) are denoted by $u(x,t)$ and $u_n(x,t)$, respectively, then $\mathscr{L}u_n(x_s,t)$ for $s = 1,2,\ldots,N$ and $\lim_{n\to\infty} u_n(x,t) = u(x,t)$.*

Let $\mathcal{P}(x)$ be the Lagrange interpolation function for approximating $u(x)$.based on interpolation remainder theorem, we get

$$\varepsilon(x) := u(x) - \mathcal{P}(x) = \frac{u^{k+1}(\tau_i)}{(k+1)!}\prod_{i=0}^{k}(x - x_i).$$

Based on the above estimates, the following results are given.

Lemma 2.2 *[33]. If $u(x) \in C^{k+1}([a,b])$, then the estimates for function $\varepsilon(x)$ is defined as*

$$\begin{cases} |\varepsilon(x)| \le C_1 \|u^{(k+1)}\|_\infty \left(\frac{\varepsilon h_x}{2k}\right)^k, \\ |\varepsilon'(x)| \le C_1^* \|u^{(k+1)}\|_\infty \left(\frac{\varepsilon h_x}{2(k-1)}\right)^{k-1}, \\ |\varepsilon''(x)| \le C_1^{**} \|u^{(k+1)}\|_\infty \left(\frac{\varepsilon h_x}{2(k-2)}\right)^{k-2}, \end{cases} \tag{7}$$

where C_1, C_1^*, C_1^{**} are constants which are independent of x, εdenotes a natural algorithm, and h_x stands for the length of $[a,b]$

Also, for two-dimensional case, if $\mathcal{P}(x,y)$ is the Lagrange interpolation function of $u(x,y)$ which satisfies $\mathcal{P}(x_k,y_n) = u(x_k,y_n)$. Then we define the error function as

$$\begin{aligned} \varepsilon(x,y) :&= u(x,y) - \mathcal{P}(x_k,y_n) \\ &= u(x,y) - \mathcal{P}(x_k,y) + \mathcal{P}(x,y) - \mathcal{P}(x_k,y_n) \\ &= \frac{\partial_x^{(k+1)} u(\tau_i,y)}{(k+1)!}\prod_{i=0}^{k}(x-x_i) + \frac{\partial_y^{(n+1)} u(x_k,\tau_j)}{(n+1)!}\prod_{j=0}^{n}(y-y_j) \end{aligned} \tag{8}$$

Then we present the following results.

Theorem 2.3 *[34]. Suppose $u \in C^0([0,T])$, $C^{\bar{k}+1}([a,b]\times[c,d])$, where $\bar{k} = \max\{k,n\}$, let $u(x_k,y_n,t) : \prod u(x_k,y_n,t) = 0$ and assume the function $f(u)$ satisfies the Lipschitz condition, we obtain*

$$\begin{aligned} |u(x,y,t) - u(x_k,y_n,t)| \le\ & C_1^{**} \left\| \partial_x^{(k+1)} u \right\|_\infty \left(\frac{\varepsilon h_x}{2(M-2)} \right)^{M-2} \\ & + C_2^{**} \left\| \partial_y^{(n+1)} u \right\|_\infty \left(\frac{\varepsilon h_y}{2(N-2)} \right)^{N-2}. \end{aligned} \tag{9}$$

Methods of approximation in space and time

Generally speaking, the nature of time-dependent reaction-diffusion equations permit the use of different numerical methods in space and time. For instance, the authors in [14,22,35–40] applied finite difference, finite element and spectral methods to discretize a range of reaction-diffusion problems in space, and the resulting systems of ODEs was advanced with different explicit time solvers. Hence, this paper applied both the spectral interpolation collocation method and the barycentric interpolation collocation method in space. The resulting systems of ODEs is advanced in time with the novel exponential time-differencing Runge-Kutta scheme [11].

Spectral interpolation collocation method (SICM)

In this segment, the kth order spectral differential matrix is adapted to discretize equation of the form (1). By following the idea in [32], we write the interpolation function $\mathcal{P}_N u(x)$ of the sequence $u_1, u_2, \ldots, u_N$ as

$$u(x) \sim \mathcal{P}_N u(x) = \sum_{m=1}^{N} u_m \Phi_N(x - x_m) \tag{10}$$

where

$$\Phi_N(x) = \frac{\sin(\pi x/h)}{\tan(x/2)(L/h)}, \quad L \gg 0,$$

P_N denotes the interpolation operator for any function $u(x)$ in interval $[0,L]$, $u_n = u(nh)$, $n = 1,2,\ldots,N, x_n - x_m = (n-m)h$, we span the interpolation space $\{\Phi_N(x-nh),\ n = 1,2,\ldots,N\}$.

At point $x_n = nh$, the expression for the kth derivative of operator $P_N u(x)$ can be derived as

$$P_N u^{(k)}(x_n) = \sum_{m=1}^{N} u_m \Phi_N^{(k)}(x_n - x_m)$$

where we denote

$$\mathcal{D}_N^{(k)}(x_n) = [\Phi_N^{(k)}(x_n - x_m)]_{n,m=1,2,\ldots,N}$$

Working in two-dimensional space, we consider a square spatial domain size $\Omega = [0, L] \times [0, L]$, and define the space grid points N_2 over Ω as

$$(x_i, y_n) = (ih, nh), \quad i, n = 1, 2, \ldots, N$$

where step size $h = L/h$ for $N \in \mathbb{N}$. By applying (10), the interpolation function $P_N u(x, y, t)$ of function $u(x, y, t)$ becomes

$$u(x, y, t) \sim P_N u(x, y, t) = \sum_{i=1}^{N} \sum_{n=1}^{N} \Phi_N(x - x_i)\Phi_N(y - y_i)u(x_i, y_n, t)$$

with $u_{i,n} = u(x, y, t), \quad i, n = 1, 2, \ldots, N$. Then at collocation points (x_a, y_b), the following relations hold:

$$u(x_a, y_b, t) \sim P_N u(x_a, y_b, t) = \sum_{i=1}^{N} \sum_{n=1}^{N} \Phi_N(x_a - x_i)\Phi_N(y_b - y_i)u(x_i, y_n, t) \tag{11}$$

Bear in mind that the second-order spatial derivatives in the directions x and y and time t is expressed as

$$\frac{\partial^2 u(x_a, y_b, t)}{\partial x^2} = u^{(2,0)}(x_a, y_b, t) \sim P_N u^{(2,0)}(x_a, y_b, t) = \sum_{i=1}^{N} \sum_{n=1}^{N} \Phi_N^{(2)}(x_a - x_i)\Phi_N(y_b - y_i)u(x_i, y_n, t)$$

and

$$\frac{\partial^2 u(x_a, y_b, t)}{\partial y^2} = u^{(0,2)}(x_a, y_b, t) \sim P_N u^{(0,2)}(x_a, y_b, t) = \sum_{i=1}^{N} \sum_{n=1}^{N} \Phi_N(x_a - x_i)\Phi_N^{(2)}(y_b - y_i)u(x_i, y_n, t).$$

It should be noted that

$$u = [u_{11}, u_{21}, \ldots, u_{N1}, u_{12}, u_{22}, \ldots, u_{N2}, u_{1N}, \ldots, u_{NN}]^T \tag{12}$$

In matrix form, Eq. (11) can be written as

$$u^{(2,0)} = \mathcal{D}_N^{(2,0)} u, \qquad u^{(0,2)} = \mathcal{D}_N^{(0,2)} u \tag{13}$$

where

$$\mathcal{D}_N^{(2,0)} u = \mathcal{D}_N^{(2)} \otimes E_N, \mathcal{D}_N^{(0,2)} u = E_N \otimes \mathcal{D}_N^{(2)}, \mathcal{D}_N^{(0,0)} = E_N \otimes E_N \tag{14}$$

where $\otimes$ is the usual matrix Kronecker product, and E_N denotes $N-$order unit matrix.

When (12) and (13) is applied to multicomponent system (2) with $i = 1, 2$, we have

$$\frac{\partial}{\partial t}\begin{pmatrix} u_1 \\ v_2 \end{pmatrix} = \begin{pmatrix} d_1\mathcal{D} & 0 \\ 0 & d_2\mathcal{D} \end{pmatrix}\begin{pmatrix} u_1 \\ u_2 \end{pmatrix} = \begin{pmatrix} f_1(u_1, u_2) \\ f_2(u_1, u_2) \end{pmatrix} \tag{15}$$

Note that

$$[u_1, u_2] = [u_{1,11}, \ldots, u_{1,N1}, u_{1,12}, \ldots, u_{1,N2}, u_{1,1N}, \ldots, u_{1,NN}]$$

$$\mathcal{D} = \mathcal{D}_N^{(2,0)} + \mathcal{D}_N^{(0,2)} = \mathcal{D}_n^{(2)} \otimes E_N + E_N \otimes \mathcal{D}_N^{(2)}$$

Similarly for the reaction term vector, we have

$$f_1(u_1, u_2), f_2(u_1, u_2) = [f_1(u_{1,11}, u_{2,11}), \ldots, f_1(u_{1,NN}, u_{2,NN}), f_2(u_{1,11}, u_{2,11}), \ldots, f_2(u_{1,NN}, u_{2,NN})].$$

Barycentric interpolation collocation method (BICM)

For the discretization scheme here, we choose a rectangular domain size $\Omega = [a, b] \times [c, d]$, these two intervals are partitioned into $M + 1, N + 1$ distinct Chebyshev nodes $a = x_0 < x_1 < \cdots < x_M = b, c = y_0 < y_1 < y_2 < \cdots < y_N = d$. By following [34] we denote $u(x_i, y, t) = u_i(y, t), i = 0, 1, 2, \ldots, M$ and fix variable y. In barycentric interpolation form, one can write the unknown function $u(x, y, t)$ as

$$u(x, y, t) = \sum_{n=0}^{M} \varphi_n(x) u_n(y, t), \tag{16}$$

where $\varphi_n(x)$ is the basis function in the $x-$direction. By using (16) in (1) or one-component case of system (2) at the nodes $x_i, i = 0, 1, 2, \ldots, M$, we obtain

$$\sum_{n=0}^{M} \varphi_n(x_i) \frac{\partial u_n(y,t)}{\partial t} - \sum_{n=0}^{M} \varphi_n''(x_i) u_n(y,t) - \sum_{n=0}^{M} \varphi_n(x_i) \frac{\partial^2 u_n(y,t)}{\partial y^2} + f\left(\sum_{n=0}^{M} \varphi_n(x_i) u_n(y,t) \right) = 0. \tag{17}$$

where

$$\varphi_n''(x_i) = \frac{d^2 \varphi_n(x_i)}{dx^2} = D_{in}^{(2)}.$$

Conveniently, the above equation can be transformed into matrix of the form

$$\begin{pmatrix} \frac{\partial u_0(y,t)}{\partial t} \\ \frac{\partial u_1(y,t)}{\partial t} \\ \vdots \\ \frac{\partial u_M(y,t)}{\partial t} \end{pmatrix} - \begin{pmatrix} D_{00}^{(2)} & D_{01}^{(2)} & \cdots & D_{0M}^{(2)} \\ D_{10}^{(2)} & D_{11}^{(2)} & \cdots & D_{1M}^{(2)} \\ \vdots & \vdots & & \vdots \\ D_{M0}^{(2)} & D_{M1}^{(2)} & \cdots & D_{MM}^{(2)} \end{pmatrix} \begin{pmatrix} u_0(y,t) \\ u_1(y,t) \\ u_M(y,t) \end{pmatrix} - \begin{pmatrix} \frac{\partial^2 u_0(y,t)}{\partial y^2} \\ \frac{\partial^2 u_1(y,t)}{\partial y^2} \\ \vdots \\ \frac{\partial^2 u_M(y,t)}{\partial y^2} \end{pmatrix} + \begin{pmatrix} f(u_0(y,t)) \\ f(u_1(y,t)) \\ \vdots \\ f(u_M(y,t)) \end{pmatrix} = 0 \tag{18}$$

In the same manner, let $u_i(y_k, t) = u_{ik}$. This implies that $u_i(y,t)$ has the barycentric interpolation of the form

$$u_i(y,t) = \sum_{j=0}^{N} \Psi_j(y) u_{ij}(t), \tag{19}$$

$\Psi_j(y)$ in the barycentric interpolation stands for the basis function on $y-$direction. By substituting for (19) in (18) at the nodes $y_k, k = 0, 1, 2, \ldots, N$, one-component form of (2) results to the following system of ordinary differential equations

$$\begin{pmatrix} \sum_{j=0}^{N} \Psi_j(y_k) \frac{\partial u_0(y,t)}{\partial t} \\ \sum_{j=0}^{N} \Psi_j(y_k) \frac{\partial u_1(y,t)}{\partial t} \\ \vdots \\ \sum_{j=0}^{N} \Psi_j(y_k) \frac{\partial u_M(y,t)}{\partial t} \end{pmatrix} - \begin{pmatrix} D_{00}^{(2)} & D_{01}^{(2)} & \cdots & D_{0M}^{(2)} \\ D_{10}^{(2)} & D_{11}^{(2)} & \cdots & D_{1M}^{(2)} \\ \vdots & \vdots & & \vdots \\ D_{M0}^{(2)} & D_{M1}^{(2)} & \cdots & D_{MM}^{(2)} \end{pmatrix} \begin{pmatrix} \sum_{j=0}^{N} \Psi_j(y_k) u_{0j}(t) \\ \sum_{j=0}^{N} \Psi_j(y_k) u_{1j}(t) \\ \vdots \\ \sum_{j=0}^{N} \Psi_j(y_k) u_{Mj}(t) \end{pmatrix} - \begin{pmatrix} \sum_{j=0}^{N} \Psi_j''(y_k) u_{0j}(t) \\ \sum_{j=0}^{N} \Psi_j''(y_k) u_{1j}(t) \\ \vdots \\ \sum_{j=0}^{N} \Psi_j''(y_k) u_{Mj}(t) \end{pmatrix} + \begin{pmatrix} f\left(\sum_{j=0}^{N} \Psi_j(y_k) u_{0j}(t)\right) \\ f\left(\sum_{j=0}^{N} \Psi_j(y_k) u_{1j}(t)\right) \\ \vdots \\ f\left(\sum_{j=0}^{N} \Psi_j(y_k) u_{Mj}(t)\right) \end{pmatrix} = 0 \tag{20}$$

where

$$\Psi_j''(y_k) = \frac{d^2 \Psi_j(y_k)}{dy^2} = D_{jk}^{(2)}.$$

Finally, we write (20) in matrix form

$$\frac{d\mathbf{U}}{dt} - (\mathcal{D}^{(2)} \otimes \mathbf{I}_N)\mathbf{U} - (\mathbf{I}_M \otimes \mathbf{D}^{(2)})\mathbf{U} + \mathbf{f}(\mathbf{U}) = 0 \tag{21}$$

where

$$\begin{aligned} \mathbf{U} &= [\mathbf{u}_0^T(t), \mathbf{u}_1^T(t), \mathbf{u}_2^T(t), \ldots, \mathbf{u}_M^T(t)]^T, \\ &= [u_{00}(t), u_{01}(t), \ldots, u_{0N}(t), u_{10}(t), u_{11}(t), \ldots, u_{1N}(t), \cdots, u_{M0}(t), u_{M1}(t), \ldots, u_{MN}(t)]^T, \\ \mathbf{u}_i(t) &= [u_{i0}(t), u_{i1}(t), \ldots, u_{iN}(t)]^T, \end{aligned}$$

$\mathcal{D}^{(2)}$ is the second-order differential matrix on equally spaced nodes $x_0, x_1, x_2, \ldots, x_M$, while $\mathbf{D}^{(2)}$ represents second-order differential matrix in the y-direction with nodes $y_0, y_1, y_2, \ldots, y_N$. $\mathbf{I}_M$ and $\mathbf{I}_N$ are the identity matrices with orders $M+1$ and $N+1$, respectively. And, $\otimes$ remains as earlier defined. It should be noted that at this stage, any explicit solver can be applied to advance in time.

Exponential time-differencing Runge-Kutta method

The explicit numerical method considered in this work is exponential time-difference (ETD) scheme of Runge-Kutta type which are known for a long time in the field of computational electrodynamics [41], a detailed review of the class of ETD schemes and their history can be found in [42]. Ever since its inception, a lot of research attention has been paid to its formulation and application to solve a range of real-life phenomena [11,22]. The idea of exponential time-differencing methods is similar to that of the Integrating factor method in the sense that both sides of a differential equation is multiplied by the integrating factor. To allow the solution of the linear part, a change of variable is made and any numerical method of interest is applied to transform nonlinear part.

When system (1) is discretized in space,it results to system of ODEs of the form

$$u_t = \mathbf{L}u + \mathbf{F}(u,t). \tag{22}$$

Next, we multiply the above equation with the integrating factor term $e^{-\mathbf{L}t}$ to yield

$$e^{-\mathbf{L}t}u_t = e^{-\mathbf{L}t}\mathbf{L}u + e^{-\mathbf{L}t}\mathbf{F}(u,t), \tag{23}$$

or

$$e^{-\mathbf{L}t}u_t - e^{-\mathbf{L}t}\mathbf{L}u = e^{-\mathbf{L}t}\mathbf{F}(u,t). \tag{24}$$

If we let $v_t = e^{-\mathbf{L}t}u_t - e^{-\mathbf{L}t}\mathbf{L}u$, then (24) becomes

$$v_t = e^{-\mathbf{L}t}\mathbf{F}(v,t). \tag{25}$$

Obviously, at this stage the stiff linear part is vanished, which means any time-stepping method of choice can be applied. For the modified ETD case, instead of changing the variable, we follow description in [22] and integrate (24) over a single time-step h to have

$$u_{n+1} = e^{\mathbf{L}h}u_n + e^{\mathbf{L}h}\int_0^h e^{-\mathbf{L}\xi}\mathbf{F}(u(t_n+\xi),t_n+\xi)d\xi. \tag{26}$$

Now, various ETD schemes can be obtained depending on how one approximates the integral (26). In [11], the authors formulated a set of schemes based on Runge-Kutta time solver,which are popularly referred to as the ETDRK schemes. In this paper only the third-order scheme, denoted as ETD3RK is considered as:

$$\begin{aligned}
\phi_n &= u_n e^{\mathbf{L}h/2} + \left(e^{\mathbf{L}h/2}-1\right)\mathbf{F}_n/\mathbf{L},\\
\varphi_n &= u_n e^{\mathbf{L}h} + \left(e^{\mathbf{L}h}-1\right)(2\mathbf{F}(\phi_n, t_n+h/2) - \mathbf{F}_n)/\mathbf{L},\\
u_{n+1} &= u_n e^{\mathbf{L}h} + \Big\{((\mathbf{L}^2h^2 - 3\mathbf{L}h + 4)e^{\mathbf{L}h} - \mathbf{L}h - 4)\mathbf{F}_n\\
&\quad +4((\mathbf{L}h-2)e^{\mathbf{L}h} + \mathbf{L}h + 2)\mathbf{F}(\phi_n, t_n+h/2)\\
&\quad +((-\mathbf{L}h+4)e^{\mathbf{L}h} - \mathbf{L}^2h^2 - 3\mathbf{L}h - 4)\mathbf{F}(\varphi_n, t_n+h)\Big\}/(\mathbf{L}^3h^2).
\end{aligned} \tag{27}$$

where terms ϕ_n and φ_n is used for the approximation of u-values at points $t_n + h/2$ and $t_n + h$, respectively. The time-stepping formula (27) is the quadrature method for integral (26) which is derived from quadratic interpolation via the points $t_n, t_n + h/2$ and $t_n + h$. Details of stability and convergence properties of ETD schemes can be found in [22,43,44].

To test the accuracy and applicability of the SICM and BICM when used in conjunction with the ETD3RK method, we consider the following problem

$$-u''(x) + \beta u(x) = f(x), \quad x \in [0,1],\ u(0) = u(1) = 0. \tag{28}$$

Here function f and real number β are assigned in such a way that there exists a unique solution. Equation (28) has been used to model a number of phenomena, for instance the concentration of chemical species transported in a fluid with velocity β. With $f(x) = \cos(\alpha\pi x)$ we compute the numerical result of the convection-diffusion equation in Fig. 1(a). In plot (b) we compute the absolute error with $f(x) = (\pi^2 + 130)\sin(\pi x)\cos(10x) + 20\pi\cos(\pi x)\sin(10x)$, the true solution is given as $U_e = \sin(\pi x)\cos(10x)$. It is obvious that both schemes compete very well with the exact solution. Absolute error results computed for different N and step-size h is presented in Table 1.

Numerical experiments

The aim of this section is based on the numerical solution of time-dependent reaction-diffusion equations, using the numerical methods as derived in Section 3. A range of nontrivial problems of reaction-diffusion systems which are still of current and recurring interests are taken from literature is chosen to demonstrate the effectiveness of the numerical schemes in one and high dimensions. All computations are carried out in MATLAB R2013a software package.

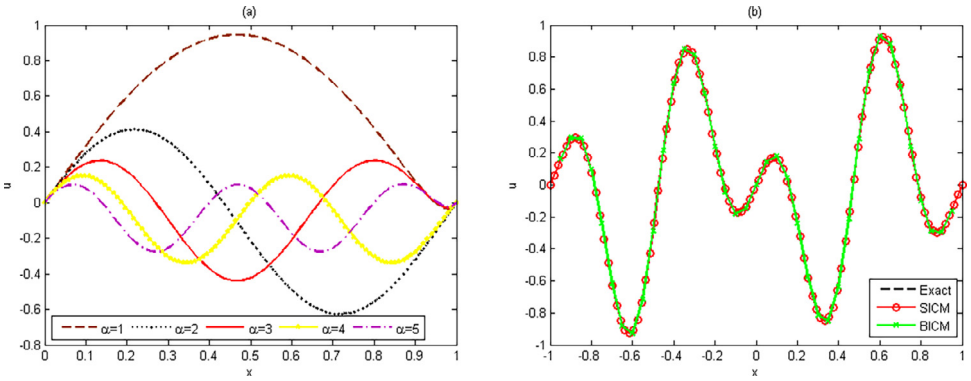

Fig. 1. Solution of problem (28) showing the performance of the schemes.

Table 1
Absolute errors for problem (28) for different step-size h and N with $\beta = 25$.

N	h	SICM	CPU	BICM	CPU
64	0.25	2.961684e-06	0.14s	1.039433e-06	0.16s
	0.125	2.284839e-07	0.13s	2.266685e-07	0.14s
	0.0625	2.539635e-07	0.12s	1.361448e-07	0.11s
128	0.25	1.316938e-06	0.12s	7.207915e-06	0.13s
	0.125	1.678102e-07	0.13s	9.258809e-07	0.11s
	0.0625	1.934009e-07	0.15s	6.645236e-07	0.12s

Bistable Allen-Cahn equation

The bistable Allen-Cahn equation is an example of time-dependent nonlinear reaction-diffusion equation

$$u_t = \gamma u_{xx} + u - u^3, \quad (x, y, z) \in \Omega, \ t > 0, \quad \frac{\partial u}{\partial \mathbf{n}}|_{\partial\Omega} = 0, \tag{29}$$

where the second-order spatial derivative is expressed in one, two and three dimensions as $u_{xx} = \frac{\partial^2 u}{\partial x^2}$, $u_{xx} = \left(\frac{\partial^2 u}{\partial x^2} + \frac{\partial^2 u}{\partial y^2}\right)$ and $u_{xx} = \left(\frac{\partial^2 u}{\partial x^2} + \frac{\partial^2 u}{\partial y^2} + \frac{\partial^2 u}{\partial z^2}\right)$, respectively.

Ever since the introduction of Allen-Cahn equation in 1979 by Allen and Cahn [45], it has been used to model a number of useful phenomena in image analysis, crystal growth, curvature flow rate, and also to model a number of biological populations [46–48]. Equation (29) has three steady states, $u^- = -1, u^0 = 0$ and $u^+ = 1$. Obviously, the middle state refers to extinction and unstable, but the two feasible or nontrivial states $u = \pm 1$ are attracting which make solutions to exhibit flat areas. Though the dynamic behavior of this equation depends on the choice of initial conditions. In the experiment, we shall explore various dynamical structures for different instances of initial conditions in one and high dimensions.

Consider 1D Allen-Cahn equation in $\Omega = [-L, L]$ for $L \gg 0$ chosen to allow the waves to propagate with simulation parameters $\gamma \in (0.1, 1)$, $\Delta t = 0.125, N = 200$. We allow initial condition to be varied as shown in the figures captions. In Fig. 2(a), the boundary condition is clamped to the extremes of domain $\Omega = [-1, 1]$ with initial condition computed as

$$u_0 = 0.53x(2 : \omega - 1) + 0.47\sin(-1.5\pi x(2 : \omega - 1)), \tag{30}$$

where ω is the length of $x \in [-1, 1]$ with $\gamma = 0.5$. Simulation runs for $t = 100$. In plot (b) the effect of diffusion coefficient γ is observed using the initial condition

$$u_0 = (x < -1)\exp(7(x + 1)) + (x > 1)\exp(-7(x - 1)) + sech(7x)^2, \tag{31}$$

with $L = 3$. Plots (c) and (d) correspond to $\gamma = 0.1$ and $\gamma = 0.45$, respectively with

$$u_0 = 0.53x + 0.47sin(-1.5\pi x) - x \tag{32}$$

on $\Omega = [-1, 1] \times (0, T]$ in order to mimic the existing behavior of the dynamic equation. We further verify the sensitivity of the Allen-Cahn equation to initial functions as displayed in Fig. 3. Numerical results in plots (a-d) correspond to the computed initial conditions

```
(a): u0=1/2*c*(sech(sqrt(c)/2*(x+8))).^2;
(b): u0=sin(32*pi);
(c): u0=exp((x/5)-1).*sin(3*pi*x/10).^2;
(d): u0=(x\lt -1).*exp(6*(x+1))+(x\gt 1).*exp(-6*(x-1))+sech(6*x).^2;
```

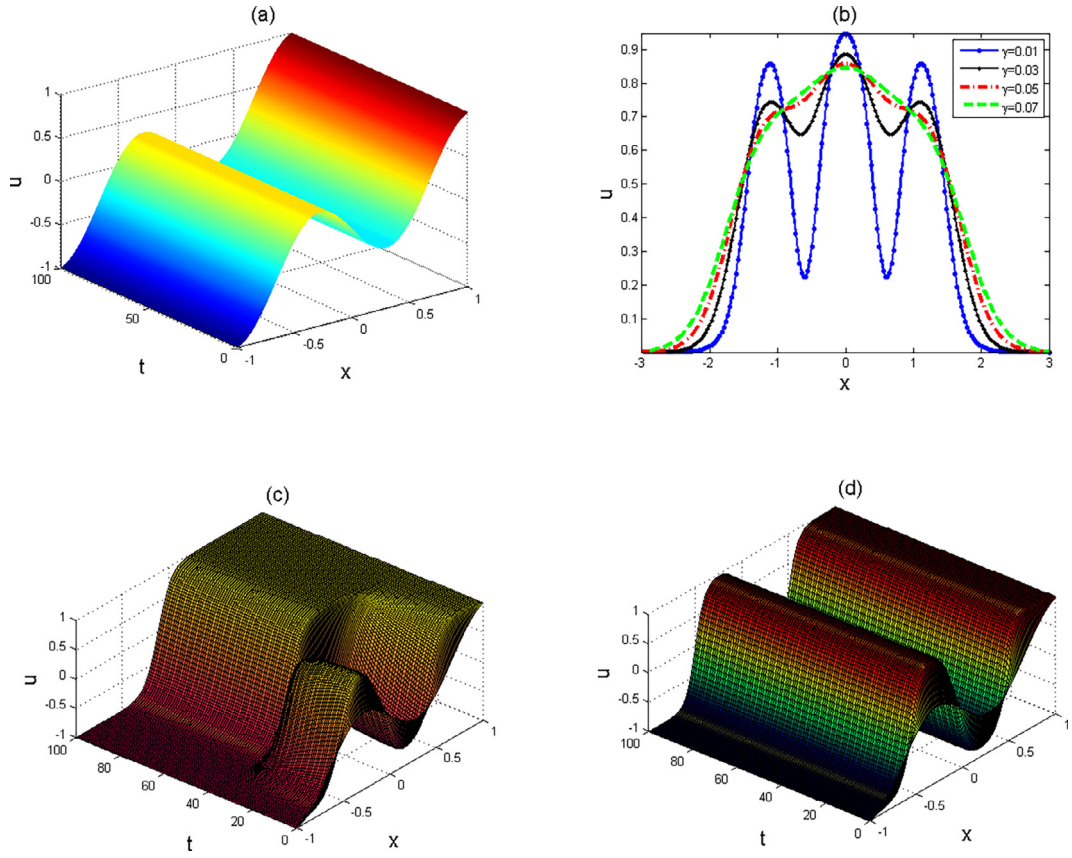

Fig. 2. One-dimensional spatiotemporal evolution of Eq. (29) for different initial conditions.

As an extension to one-dimensional experiments, we consider 2D Allen-Cahn equation on different computational domain $\Omega = [-L, L] \times [-L, L] \times [0, T]$ subject to various initial conditions to see the effect of computational time and diffusion coefficient γ. In Fig. 4, we utilized parameters $\gamma = 0.5, L = 10, h = 0.01, N = 256$, with initial conditions taken as

$$u_0 = 10\exp(-10((x-5)^2 + (y-5)^2)) + 10\exp(-10((x+5)^2 + (y+5)^2)) \\ +10\exp(-10((x-2)^2 + (y+2)^2)) + 10\exp(-10((x+2)^2 + (y-2)^2)), \tag{33}$$

and

$$u_0 = 10\exp(-10((x+2)^2 + (y+4)^2)) + 10\exp(-10((x-2)^2 + (y-2)^2)) \\ +10\ exp(-15((x+2)^2 + (y-4)^2)) \tag{34}$$

which lead to the generation of three- and four-solitons (pulses), respectively at initial stage and as simulation time progresses, the standing solitons merged gradually as one with a large crater at the top. Solitons or pulse formation process has a lot of applications in optic fiber (due delicate balance between nonlinear and linear effects in the medium), and laser (where pulses of well-defined shape and width are generated). Pulse splitting process is also an important phenomena for pattern formation in applied chemistry, physics and biology. More periodic pulse formation is possible depending on how the initial condition is formulated.

In Fig. 5 we employ the initial condition computed as

```
u0=exp(-20*((x-rho/3).^2+(y-rho/3).^2)/rho)- {\ldots}
exp(-20*((x-rho/2).^2+(y-rho/2).^2)/rho)+{\ldots}
exp(-20*((x-rho).^2+(y-rho).^2)/rho);
```

to obtain the evolution of cyclic patterns with $rho = 7$. The upper and lower rows correspond to $\gamma = 0.01, 0.50$, respectively. Since Allen-Cahn equation has been used to model spatial distribution of biological populations, to mimic the behavior in ecological perspective, we allow the initial condition to evolve naturally by utilizing the computer randomly perturbed condition

$$u_0(x, y, 0) = randn(N, N) * 0.5$$

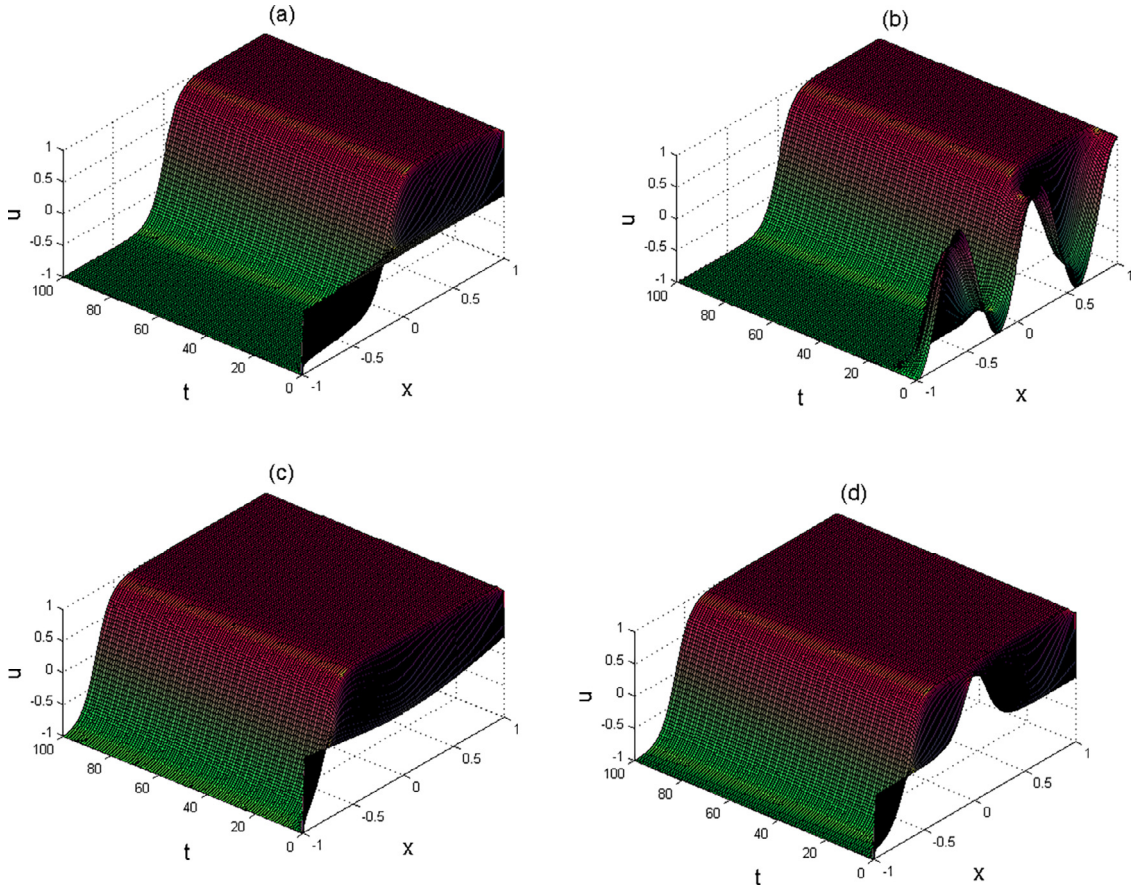

Fig. 3. One-dimensional evolution of model (29) showing the sensitivity to various initial conditions.

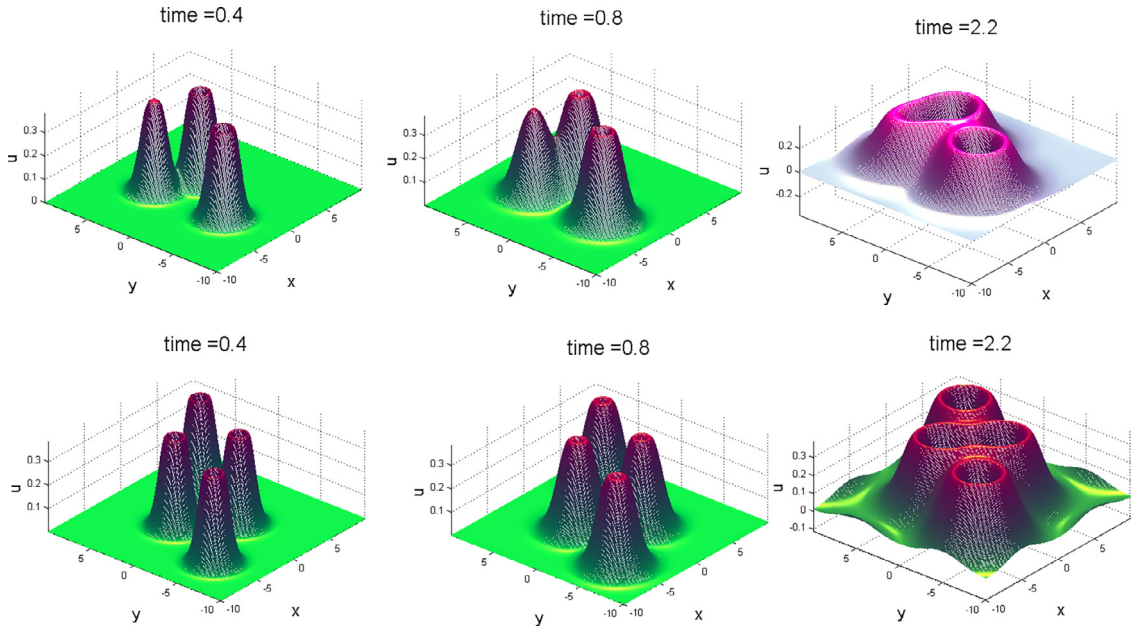

Fig. 4. Two-dimensional distribution of Allen-Cahn equation for different computational time and initial conditions. The upper and lower rows correspond to the emergence of the three and four solitons, respectively.

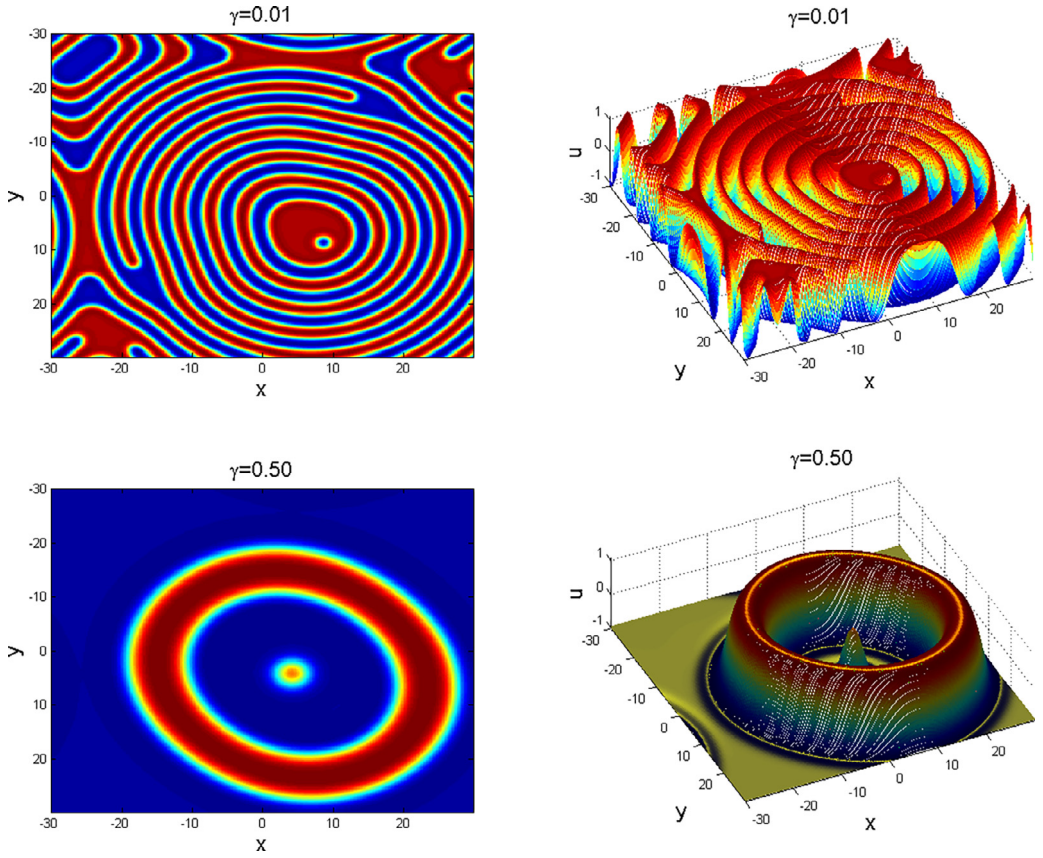

Fig. 5. Two-dimensional evolution of Eq. (29) showing cyclic patterns for different parameter γ.

where $N = 200$. The reason for this choice of initial condition arises due to a subtle fact that a random initial data often results to a solution with different wave frequencies, so that more interesting and detailed scenarios associated with various wave frequencies are explored in the dynamical process, while a numerical experiment with a smooth initial data may leads to solution with trivial structure in a short time. The upper, middle and lower rows in Fig. 6 correspond to $\gamma = 0.10, 0.50, 0.01$, respectively. In this result, we observed the evolution of Turing spirals, mitotic spots and stripe-like patterns which have application in applied and computational ecology.

In a similar fashion, we consider (29) on $\Omega = [0, L]^3 \times (0, T]$. The above initial function is extended to 3D to obtain numerical results in Fig. 7 for different γ as

```
u0=exp(-20*((x-rho/3).^2+(y-rho/3).^2+(z-rho/3).^2)/rho)- {\ldots}
exp(-20*((x-rho/2).^2+(y-rho/2).^2+(z-rho/2).^2)/rho)+{\ldots}
exp(-20*((x-rho).^2+(y-rho).^2+(z-rho).^2)/rho);
```

with parameters $N = 200, L = 100, h = 0.2$. Simulation runs for $t = 20$.

Coupled nonlinear reaction-diffusion equations

For two component reaction-diffusion example, we consider a coupled nonlinear system of equations

$$\begin{aligned} u_t &= D_u u_{xx} = f(u, v) = u(1-u) - \frac{uv}{u+\beta}, \\ v_t &= D_v v_{xx} = g(u, v) = \frac{\alpha uv}{u+\beta} - \sigma v \end{aligned} \tag{35}$$

where $u(x, t)$ and $v(x, t)$ are species of prey and predator, respectively, in position x and time t, and $D_u > 0, D_v > 0$ are the diffusion coefficients of species u and v. The functions $f(u, v)$ and $g(u, v)$ account for all the local biological processes in a particular habitat. In attempt to give a good guidelines on the right choice of parameters for numerical simulation of the full reaction–diffusion system (35), it is highly mandatory to consider the local dynamics of the system [15,49]. By considering

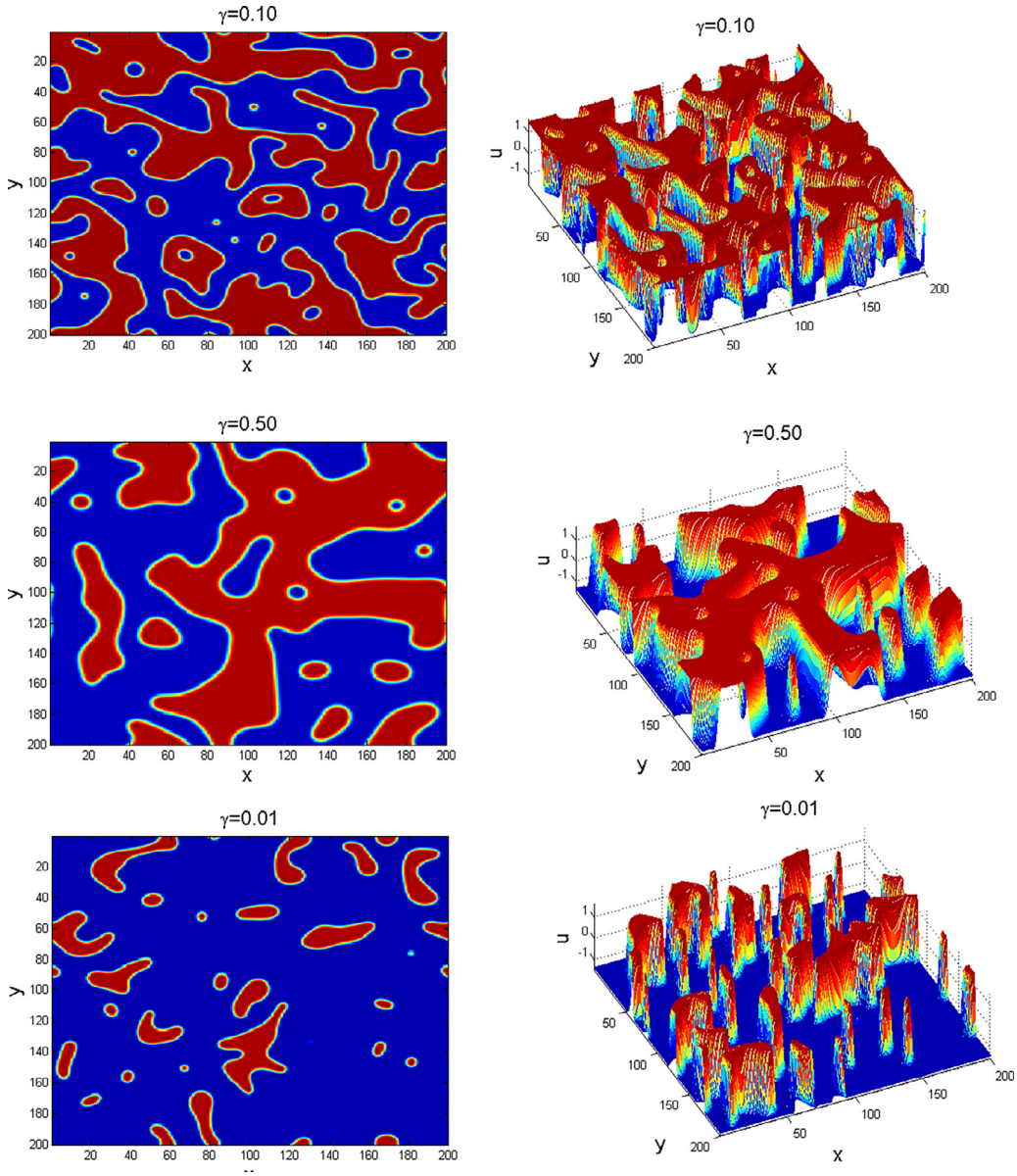

Fig. 6. The 2D chaotic evolution of (29) showing spiral patterns.

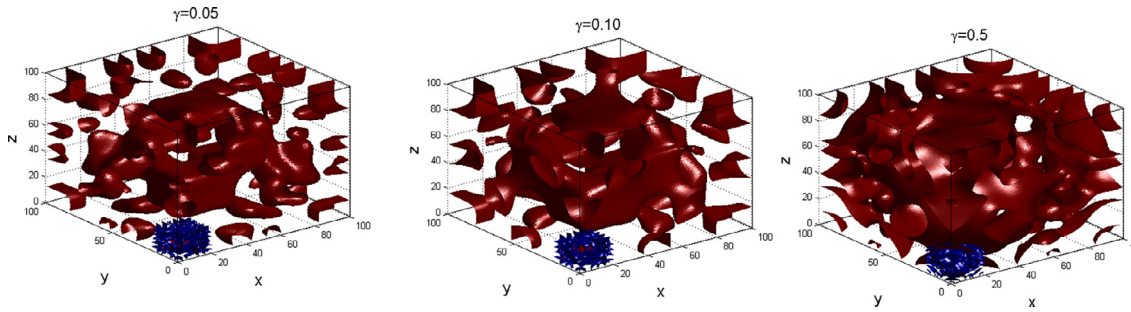

Fig. 7. Three-dimensional solution of Allen-Cahn equation for different values γ.

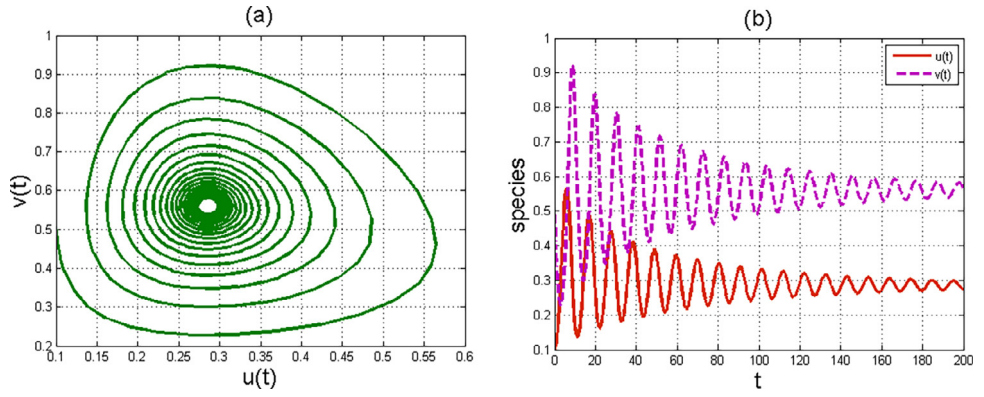

Fig. 8. Time evolution of predator-prey system (36).

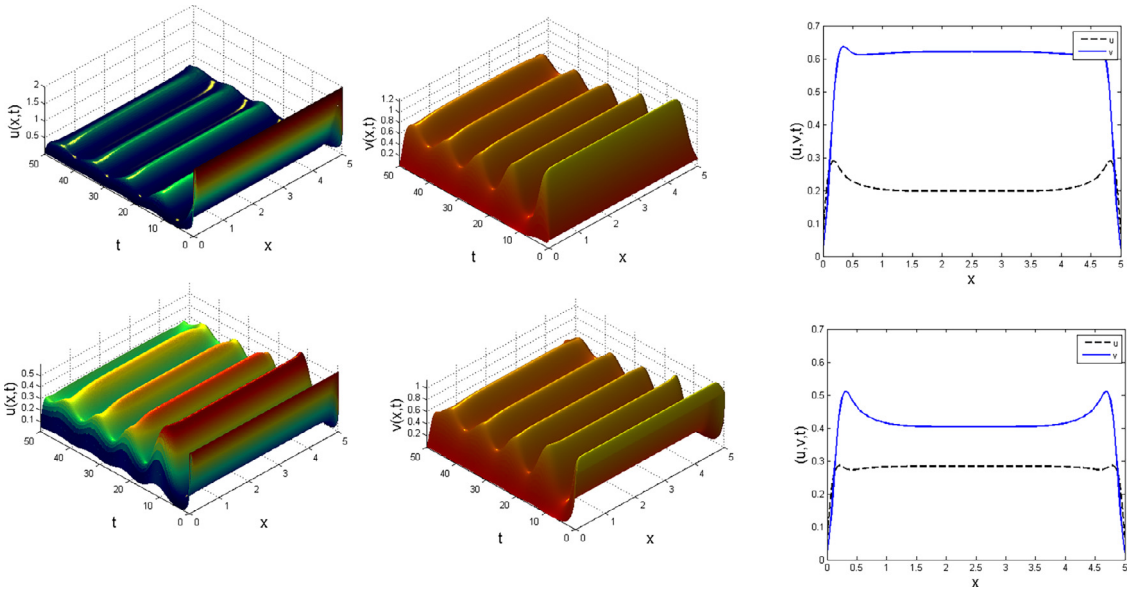

Fig. 9. One-dimensional solution of predator-prey system (35) for different initial states.

model (35) without diffusion terms, one observes by linear stability analysis that the system of equations

$$\begin{aligned} u_t &= f(u,v) = u(1-u) - \frac{uv}{u+\beta}, \\ v_t &= g(u,v) = \frac{\alpha uv}{u+\beta} - \sigma v \end{aligned} \tag{36}$$

have $E^0 = (0,0)$ (washout state), $E^1 = (1,0)$ which corresponds to the existence of only prey species, and the nontrivial state $E^* = (u*, v*)$ as the biologically meaningful state which corresponds to the existence of both prey and predator, where

$$u^* = \frac{\beta\sigma}{\alpha - \sigma}, \quad v^* = (1-u^*)(u^*+\beta)$$

with $\alpha > \sigma$ and $\beta < \frac{\alpha-\sigma}{\sigma}$. The community matrix of system (36) at point E^* is given by

$$J_{E^*} = \begin{pmatrix} 1 - 2u - \frac{\beta v^*}{(u^*+\beta)^2} & -\frac{u^*}{u^*+\beta} \\ \frac{\alpha\beta v^*}{(u^*+\beta)^2} & \frac{\alpha u^*}{(u^*+\beta)} - \sigma \end{pmatrix} \tag{37}$$

which by using the values of u^* and v^* above leads to

$$J_{E^*} = \begin{pmatrix} [(1-\beta)\alpha - (1+\beta-\beta^2)\sigma]/(\alpha-\sigma) & -\sigma/\alpha \\ (1-\beta)\alpha - \sigma & 0 \end{pmatrix}. \tag{38}$$

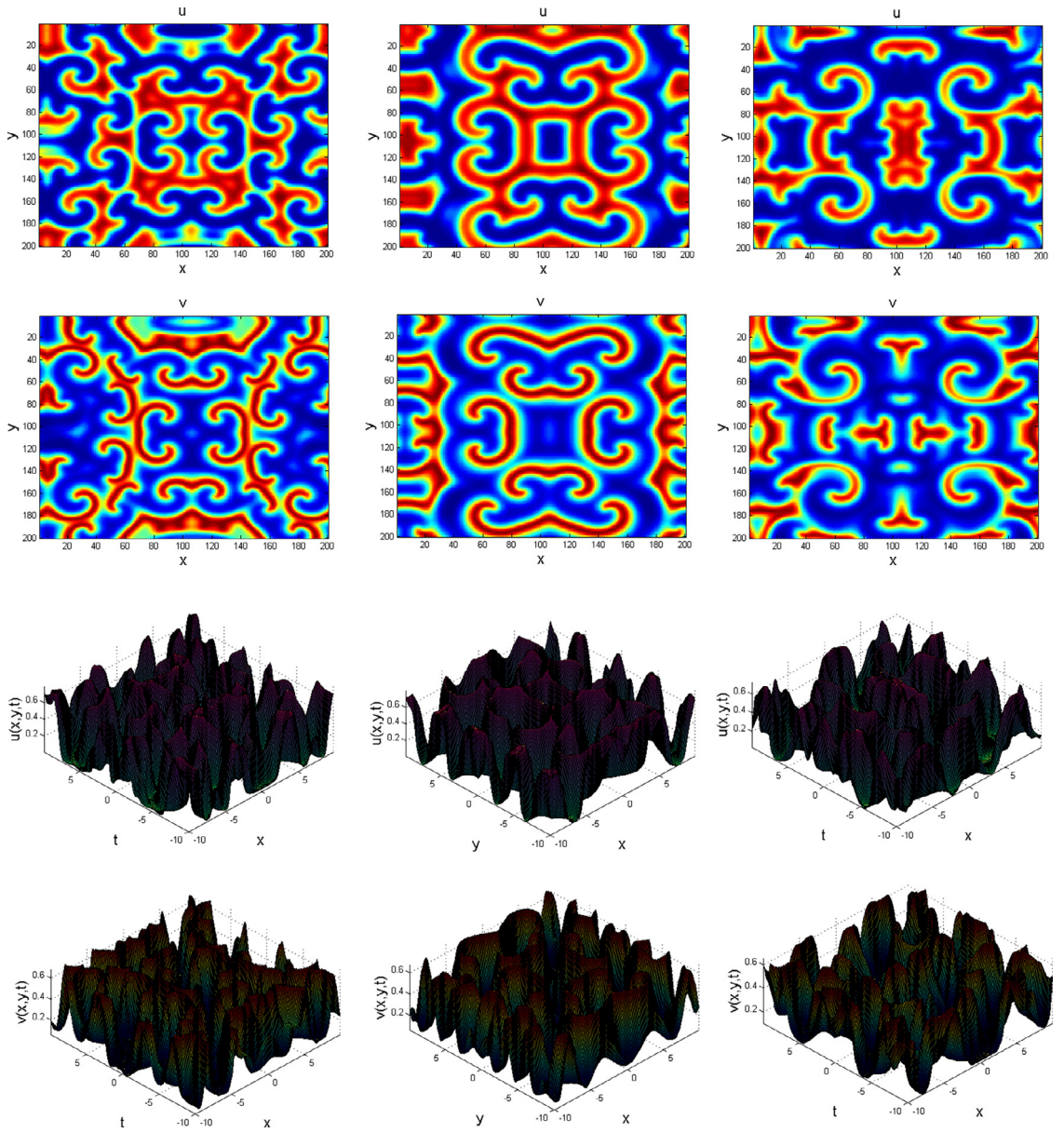

Fig. 10. Two-dimensional solution of system (35) showing spiral patterns for different values of σ. The first, second and third columns correspond to $\sigma = (0.2, 0.21, 0.24)$, respectively.

The corresponding Turing bifurcation conditions are

$$(\beta+1)\sigma < \alpha < \frac{1+\beta-\beta^2}{1-\beta}\sigma,$$

$$\alpha(\alpha-\alpha\beta-(1+\beta-\beta^2)\sigma)^2 > 4\sigma(\alpha-\alpha\beta-\sigma)(\alpha-\sigma)^2.$$

For numerical experiments, we utilize zero-flux boundary condition and parameter values $\beta = 0.2, \alpha = 1.0$ and $\sigma = 0.5$. The time evolution and corresponding species attractor for system (36) is given in Fig. 8.

For one-dimensional experiment, we apply $x \in [0, L]$, $L = 5$ and set the initial condition as

$$\begin{aligned} u(x,0) &= 1/5 + 10e-08(x-1200).*(x-2800), \\ v(x,0) &= 4/5 + 10e-08*(x-1200).*(x-2800), \end{aligned} \tag{39}$$

to obtain numerical result in Fig. 9.The upper and lower rows correspond to random initial condition and (39) It was observed that both prey and predator species oscillate in phase regardless of the variation in parameters or initial function.

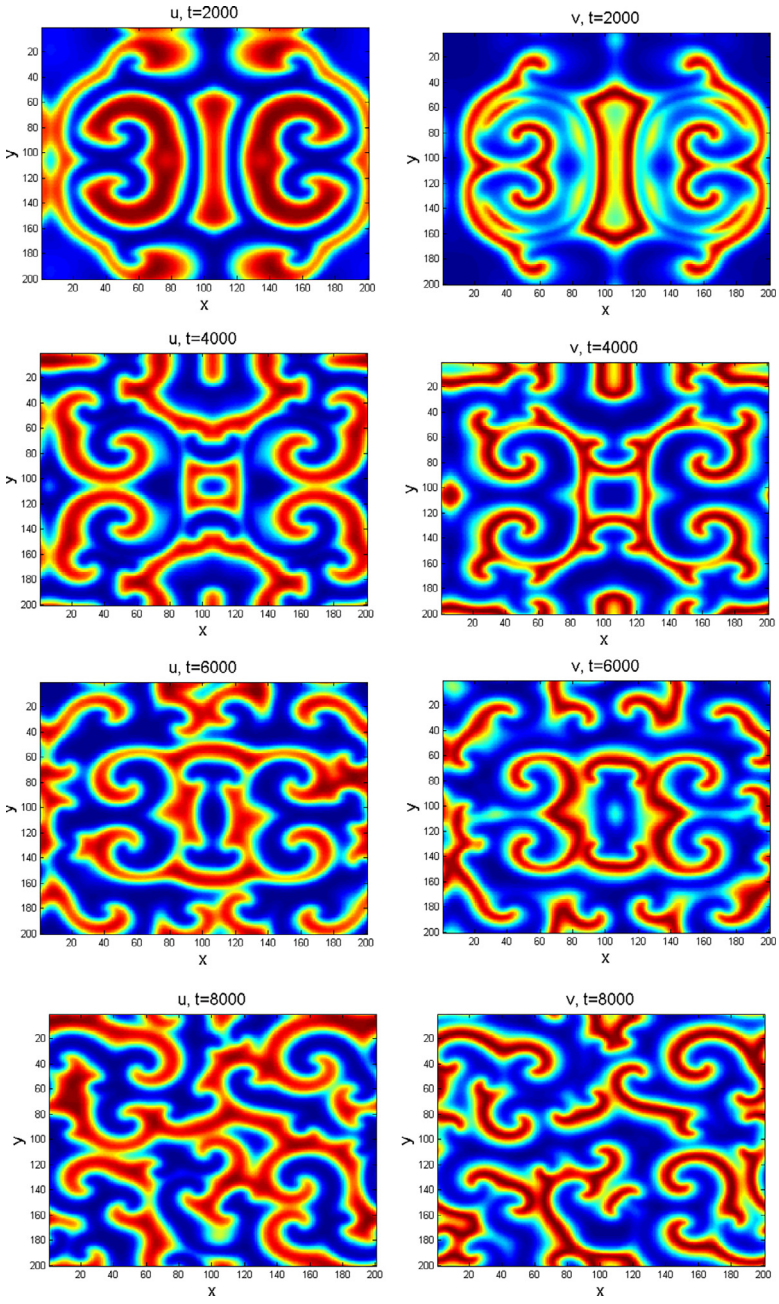

Fig. 11. Two-dimensional evolution of predator-prey system (35) showing the effects of simulation time t.

For 2D experiments, the predator-prey system is considered in $\Omega = [-L, L]$ for $L = 10$, and apply the following initial condition [37]

$$\begin{aligned} u(x, y, 0) &= 1 - \exp(-20((x - 1/2)^2 + (y - 1/2)^2)), \\ v(x, y, 0) &= \exp(-20((x - 1/2)^2 + (y - 1/2)^2)) \end{aligned} \tag{40}$$

to have the chaotic spiral patterns as displayed in Figs. 10 and 11. In Fig. 10, we allow σ to vary as shown in the caption, while the effects of increasing simulation time is displayed in Fig. 11. It should be mentioned that it is possible to obtain other Turing patterns such as spots and pure stripes, depending on the choice of initial conditions. The chaotic result obtained here has a lot of application in finance, biology and engineering.

Conclusion

The nature of reaction-diffusion equations allow the use of different methods of approximation in space and time. In this paper, a combination of the exponential time-differencing Runge Kutta method with both Spectral interpolation collocation scheme and Barycentric interpolation collocation method is considered to solve a range of system of PDEs, namely the Allen-Cahn equation and coupled nonlinear system of predation in one and high dimensions. It was observed in the simulation experiment that the spectral based scheme adapts better in conjunction with the exponential time-differencing method. A number of nonlinear phenomena such as spatiotemporal oscillation, chaotic and irregular spirals, and other Turing-like structures arising from one, two and three dimensional models are obtained. The numerical techniques reported in this work can be extended to solve multicomponents reaction-diffusion problems arising in engineering and applied sciences.

Declaration of Competing Interest

The authors declare that they have no known competing financial interests or personal relationships that could have appeared to influence the work reported in this paper.

References

[1] N. Abeye, M. Ayalew, D.L. Suthar, S.D. Purohit, K. Jangid, Numerical solution of unsteady state fractional advection–dispersion equation, Arab J. Basic Appl. Sci. 29 (2022) 77–85.
[2] R. Al-Deiakeh, O.A. Arqub, M. Al-Smadi, S. Momani, Lie symmetry analysis, explicit solutions, and conservation laws of the time-fractional fisher equation in two-dimensional space, J. Ocean Eng. Sci. 7 (2022) 345–352.
[3] M. Alqhtani, K.M. Owolabi, K.M. Saad, E. Pindza, Efficient numerical techniques for computing the Riesz fractional-order reaction-diffusion models arising in biology, Chaos Solitons Fractals 161 (2022) 112394.
[4] K.M. Owolabi, Robust and adaptive techniques for numerical simulation of nonlinear partial differential equations of fractional order, Commun. Nonlinear Sci. Numer. Simul. 44 (2017) 304–317.
[5] S. Qureshi, S. Aziz, Fractional modeling for a chemical kinetic reaction in a batch reactor via nonlocal operator with power law kernel, Physica A 542 (2019) 123494.
[6] I. Jaradat, M. Alquran, S. Qureshi, T.A. Sulaiman, A. Yusuf, Convex-rogue, half-kink, cusp-soliton and other bidirectional wave-solutions to the generalized Pochhammer-Chree equation, Phys. Scr. 97 (2022) 055203.
[7] A. Polyani, V. Zaotsev, Handbook of Nonlinear Partial Differential Equations, CRC Press, Cambridge, 2018.
[8] E. Tadmor, A review of numerical methods for non-linear partial differential equations, Bull. Am. Math. Soc. 49 (2012) 507–554.
[9] L.K. Yadav, G. Agarwal, D.L. Suthar, S.D. Purohit, Time-fractional partial differential equations: a novel technique for analytical and numerical solutions, Arab J. Basic Appl. Sci. 29 (2022) 86–98.
[10] S.D. Purohit, D. Baleanu, K. Jangid, On the solutions for generalised multiorder fractional partial differential equations arising in physics, Numer. Methods Appl. Sci. (2021), doi:10.1002/mma.7431.
[11] S.M. Cox, P.C. Matthews, Exponential time differencing for stiff systems, J. Comput. Phys. 176 (2002) 430–455.
[12] C. Klein, Fourth order time-stepping for low dispersion Korteweg-de Vries and nonlinear Schrodinger equations, Electron. Trans. Numer. Anal. 29 (2008) 116–135.
[13] K.M. Owolabi, A. Atangana, Analysis of mathematics and numerical pattern formation in superdiffusive fractional multicomponent system, Adv. Appl. Math. Mech. 9 (2017) 1438–1460.
[14] A. Bueno-Orovio, D. Kay, K. Burrage, Fourier spectral methods for fractional-in-space reaction-diffusion equations, BIT Numer. Math. 54 (2014) 937–954.
[15] M. Garvie, Finite-difference schemes for reaction-diffusion equations modeling predator-pray interactions in MATLAB, Bull. Math. Biol. 69 (2007) 931–956.
[16] K.M. Owolabi, High-dimensional spatial patterns in fractional reaction-diffusion system arising in biology, Chaos Solitons Fractals 34 (2020) 109723.
[17] E. Pindza, K.M. Owolabi, Fourier spectral method for higher order space fractional reaction-diffusion equations, Commun. Nonlinear Sci. Numer.Simul. 40 (2016) 112–128.
[18] U.M. Ascher, S.J. Ruth, B.T.R. Wetton, Implicit-explicit methods for time-dependent partial differential equations, SIAM J. Numer. Anal. 32 (1995) 797–823.
[19] W. Hundsdorfer, S.J. Ruuth, IMEX extensions of linear multistep monotonicity and boundedness properties, J. Comput. Phys. 225 (2007) 2016–2042.
[20] K.M. Owolabi, Robust IMEX schemes for solving two-dimensional reaction-diffusion models, Int. J. Nonlinear Sci.Numer. Simul. 16 (2015) 271–284.
[21] S. Krogstad, Generalized integrating factor methods for stiff PDEs, J. Comput. Phys. 203 (2005) 72–88.
[22] A. Kassam, L.N. Trefethen, Fourth-order time-stepping for stiff PDEs, SIAM J. Sci. Comput. 26 (2005) 1214–1233.
[23] K.M. Owolabi, K.C. Patidar, Higher-order time-stepping methods for time-dependent reaction-diffusion equations arising in biology, Appl. Math. Comput. 240 (2014) 30–50.
[24] G. Arora, B.K. Singh, Numerical solution of burgers' equation with modified cubic B-spline differential quadrature method, Appl. Math. Comput. 224 (2013) 166–177.
[25] N. Dhiman, M. Tamsir, A collocation technique based on modified form of trigonometric cubic B-spline basis functions for Fisher's reaction-diffusion equation, Multidiscip. Model. Mater.Struct. 14 (2018) 923–939.
[26] O. Oruc, Two meshless methods based on local radial basis function and barycentric rational interpolation for solving 2D viscoelastic wave equation, Comput. Math. Appl. 79 (2020) 3272–3288.
[27] H. Wu, Y. Wang, W. Zhang, Numerical solution of a class of nonlinear partial differential equations by using barycentric interpolation collocation method, Math. Probl. Eng. 2018 (7260346) (2018) 10.
[28] M.Y. Ansari, A.A. Shaikh, S. Qureshi, Error bounds for a numerical scheme with reduced slope evaluations, J. Appl. Environ. Biol.Sci. 8 (2018) 67–76.
[29] A. El-Ajou, O.A. Arqub, S. Momani, Approximate analytical solution of the nonlinear fractional KdV-burgers equation: a new iterative algorithm, J. Comput. Phys. 293 (2019) 81–95.
[30] O.A. Arqub, Numerical solutions for the robin time-fractional partial differential equations of heat and fluid flows based on the reproducing kernel algorithm, Int. J. Numer. Methods Heat Fluid Flow 28 (2018) 828–856.
[31] O.A. Arqub, Application of residual power series method for the solution of time-fractional schrodinger equations in one-dimensional space, Fundam. Inform. 166 (2019) 87–110.
[32] F. Liu, Y. Wang, S. Li, Barycentric interpolation collocation method for solving the coupled viscous burgers' equations, Int. J. Comput. Math. 95 (2018) 2162–2173.
[33] S.C. Yi, L.Q. Yao, A steady barycentric lagrange interpolation method for the 2D higher-order time-fractional telegraph equation with nonlocal boundary condition with error analysis, Numer. Methods Partial Differ. Equ. 35 (2019) 1694–1716.

[34] Y. Deng, Z. Weng, Barycentric interpolation collocation method based on Crank-Nicolson scheme for the Allen-Cahn equation, AIMS Math. 6 (2021) 3857–3873.
[35] K.M. Owolabi, A. Atangana, Numerical approximation of nonlinear fractional parabolic differential equations with Caputo-Fabrizio derivative in Riemann-Liouville sense, Chaos Solitons Fractals 99 (2017) 171–179.
[36] M. Calvo, C. Palencia, A class of explicit multi-step exponential integrators for semi-linear problems, Numer. Math. 102 (2006) 367–381.
[37] K.M. Owolabi, Robust and adaptive techniques for numerical simulation of nonlinear partial differential equations of fractional order, Commun. Nonlinear Sci. Numer.Simul. 44 (2017) 304–317.
[38] R.V. Craster, R. Sassi, Spectral Algorithms for Reaction-Diffusion Equations, Technical report, Note del Polo N. 99, Universitá di Milano, 2006 arXiv: 1810.07431v1.
[39] M. Garvie, C. Trenchea, Finite element approximation of spatially extended predator-prey interactions with the Holling type II functional response, Numer. Math. 107 (2007) 641–667.
[40] K.M. Owolabi, K.C. Patidar, Numerical simulations of multicomponent ecological models with adaptive methods, Theor. Biol. Med. Modell. 13 (1) (2016).
[41] A. Taflove, Computational Electrodynamics: The Finite Difference Time-Domain Method, Artech House, Boston, 1995.
[42] B. Minchev, W. Wright, A Review of Exponential Integrators for First Order Semi-Linear Problems, Technical report 2, 2005.
[43] Q. Du, W. Zhu, Stability analysis and applications of the exponential time differencing schemes, J. Comput. Appl. Math. 22 (2004) 200–209.
[44] Q. Du, W. Zhu, Analysis and applications of the exponential time differencing schemes and their contour integration modifications, BIT Numer. Math. 45 (2005) 307–328.
[45] S.M. Allen, J.W. Cahn, A microscopic theory for antiphase boundary motion and its application to antiphase domain coarsening, Acta Metall. 27 (1979) 1085–1095.
[46] M. Benes, V. Chalupecky, K. Mikula, Geometrical image segmentation by the Allen-Cahn equation, Appl. Numer. Math. 51 (2004) 187–205.
[47] X.B. Feng, A. Prohl, Numerical analysis of the Allen-Cahn equation and approximation for mean curvature flaws, Numer. Math. 94 (2003) 33–65.
[48] D.S. Cohen, J.D. Murray, A generalized diffusion model for growth and dispersal in a population, J. Math. Biol. 12 (1981) 237–249.
[49] A.B. Medvinsky, S.V. Petrovskii, I.A. Tikhonova, H. Malchow, B.-L. Li, Spatiotemporal complexity of plankton and fish dynamics, SIAM Rev. 44 (2002) 311–370.